Journal of Oceanology and Limnology
Vol. 41 No. 2, P. 729-739, 2023
https://doi.org/10.1007/s00343-022-2106-1

Spatial distribution and inventory of natural gas hydrate in the Qiongdongnan Basin, northern South China Sea*

Zhongxian ZHAO[1], Ning QIU[1, 2, **], Zhen SUN[1, 2], Wen YAN[1, 2], Genyuan LONG[3, 4, **], Pengchun LI[1, 2], Haiteng ZHUO[5]

[1] *Key Laboratory of Ocean and Marginal Sea Geology, South China Sea Institute of Oceanology, Chinese Academy of Sciences, Guangzhou 511458, China*

[2] *Southern Marine Science and Engineering Guangdong Laboratory (Guangzhou), Guangzhou 511458, China*

[3] *Hainan Key Laboratory of Marine Geological Resources and Environment, Haikou 570206, China*

[4] *Marine Geological Institute of Hainan Province, Haikou 570206, China*

[5] *School of Marine Sciences, Sun Yat-sen University, Zhuhai 519082, China*

Received Mar. 16, 2022; accepted in principle Apr. 18, 2022; accepted for publication May 27, 2022

Abstract Natural gas hydrate is a potential clean energy source and is related to submarine geohazard, climate change, and global carbon cycle. Multidisciplinary investigations have revealed the occurrence of hydrate in the Qiongdongnan Basin, northern South China Sea. However, the spatial distribution, controlling factors, and favorable areas are not well defined. Here we use the available high-resolution seismic lines, well logging, and heat flow data to explore the issues by calculating the thickness of gas hydrate stability zone (GHSZ) and estimating the inventory. Results show that the GHSZ thickness ranges between mostly ~200 and 400 m at water depths >500 m. The gas hydrate inventory is ~6.5×10^9-t carbon over an area of ~6×10^4 km^2. Three areas including the lower uplift to the south of the Lingshui sub-basin, the Songnan and Baodao sub-basins, and the Changchang sub-basin have a thick GHSZ of ~250–310 m, 250–330 m, and 350–400 m, respectively, where water depths are ~1 000–1 600 m, 1 000–2 000 m, and 2 400–3 000 m, respectively. In these deep waters, bottom water temperatures vary slightly from ~4 to 2 °C. However, heat flow increases significantly with water depth and reaches the highest value of ~80–100 mW/m^2 in the deepest water area of Changchang sub-basin. High heat flow tends to reduce GHSZ thickness, but the thickest GHSZ still occurs in the Changchang sub-basin, highlighting the role of water depth in controlling GHSZ. The lower uplift to the south of the Lingshui sub-basin has high deposition rate (~270–830 m/Ma in 1.8–0 Ma); the thick Cenozoic sediment, rich biogenic and thermogenic gas supplies, and excellent transport systems (faults, diapirs, and gas chimneys) enables it a promising area of hydrate accumulation, from which hydrate-related bottom simulating reflectors, gas chimneys, and active cold seeps were widely revealed.

Keyword: gas hydrate stability zone; gas hydrate inventory; Qiongdongnan Basin; South China Sea

1 INTRODUCTION

Gas hydrates are solid, ice-like compounds consisting of hydrocarbon (mostly methane) or nonhydrocarbon gases trapped by water molecules (Kvenvolden, 1993; Sloan and Koh, 2007). Three types of gas hydrate of cubic structures I and II, and hexagonal structure III were already found and

* Supported by the K. C. Wong Education Foundation (No. GJTD-2018-13), the Youth Innovation Promotion Association of Chinese Academy of Sciences, the Key Special Project for Introduced Talents Team of Southern Marine Science and Engineering Guangdong Laboratory (Guangzhou) (Nos. GML2019ZD0104, GML2019ZD0205), the Guangzhou Municipal Science and Technology Program (No. 201904010285), the National Natural Science Foundation of China (No. 42076077), the Innovation Academy of South China Sea Ecology and Environmental Engineering, Chinese Academy of Sciences (No. ISEE2018PY02), the National Key Research and Development Program of China (No. 2021YFC3100604), the Hainan Key Laboratory of Marine Geological Resources and Environment (No. HNHYDZZYHJKF003), the Guangdong Basic and Applied Basic Research Foundation (No. 2021A1515011298), and the Guangdong Special Support Talent Team Program (No. 2019BT02H594)

** Corresponding authors: genyuanl203@163.com; ningqiu@scsio.ac.cn

reported (Stackelberg, 1949; Ripmeester et al., 1987). Gas hydrate is widely distributed in deep marine and sub-permafrost sediments (Milkov, 2004) in gas hydrate stability zone (GHSZ) under relatively high pressure and low temperature. Due to high concentration of methane in hydrates (~170-m^3 methane for 1-m^3 structure I hydrate under standard pressure and temperature (SPT)) (Claypool and Kaplan, 1974) and large hydrogen to carbon ratio of methane (Marchetti, 1985), gas hydrates become a potential clean energy source and an important carbon reservoir. Moreover, hydrates are easily dissociated as temperature or pressure varies, which can cause methane release to induce cold seeps or trigger catastrophic submarine slides (Paull et al., 2002; Westbrook et al., 2009).

Formation of methane hydrates within GHSZ is controlled by a series of physical, bio- and thermo-chemical processes to degrade particulate organic carbon (POC) deposited on the seafloor (Fig.1). Firstly, POC is mostly degraded by microorganisms in the bioturbated layer (0–10-cm sediment depth). Then other POC is further buried below 10 cm, which is partly degraded via anaerobic microbes in the sulfate reduction zone (Flögel et al., 2011), partly degraded in the methanogenic zone to generate biogenic methane (Fig.1a), and partly buried below biosphere to decompose into gas, oil, and other high-temperature (>100 °C) products under thermo-chemical processes (Fig.1a). Biogenic and thermogenic methane are main sources for gas hydrates formed in GHSZ when methane concentration exceeds pressure, temperature, and salinity-dependent solubility limits of hydrate (Fig.1b) (Burwicz et al., 2011). However, the geothermal gradient rises too fast with depth and gas hydrates occur only in upper sediment layer shallower than ~1 km (Fig.1b) (Kvenvolden, 1993; Miles, 1995).

Gas hydrate was first discovered in high-pressure natural gas pipelines in the 1930s (Hammerschmidt, 1934), and was drilled on the Blake Outer Ridge in 1972 (Hollister et al., 1972). Thereafter, gas hydrates were widely found and several production tests were already conducted in Canadian Arctic, Alaska, and offshore Japan (Beaudoin et al., 2014). In the South China Sea region, multidisciplinary investigations also revealed occurrence of gas hydrates in offshore Taiwan Island (Liu et al., 2006; Lin et al., 2009), Zhujiang (Pearl) River Mouth Basin (Zhang et al., 2015; Qian et al., 2018; Li et al., 2020), and Qiongdongnan Basin (Jiang et al., 2021; Liao et al., 2021). Especially in the Qiongdongnan

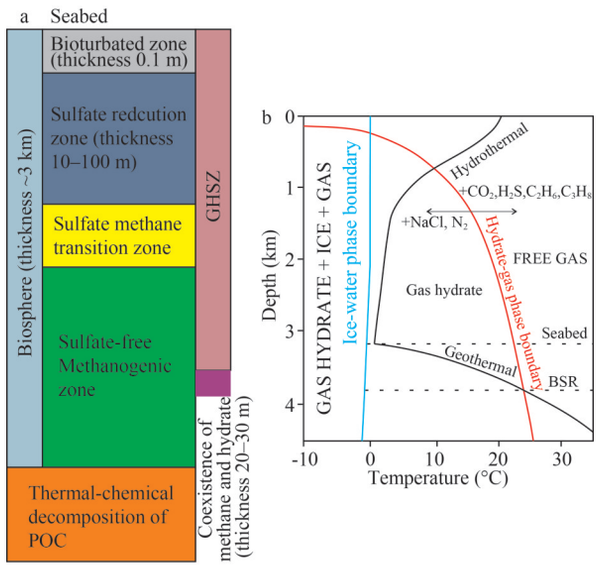

Fig.1 Formation structure of seafloor natural gas hydrates and their phase diagrams

Schematic illustration showing the formation of hydrate within gas hydrate stability zone (GHSZ) in the upper sediment layer under sufficient methane supply from methanogenic zone (biogenic methane) or below the biosphere (thermogenic methane) through degradation of buried particular organic carbon (POC) (Kvenvolden, 1993; Miles, 1995; Flögel et al., 2011) (a); phase diagrams illustrating stable zone of gas hydrates; salts in pore water can shift the gas hydrate phase boundary to the left and reduce the stable area of gas hydrates (Kvenvolden, 1993; Miles, 1995; Flögel et al., 2011) (b).

Basin, currently active "Haima" cold seeps were found by remotely operated vehicle in 2015 and 2016 (Feng et al., 2018; Zhao et al., 2020), showing abundant gas hydrate deposits. However, the spatial distribution of gas hydrates, the controlling factors, and the most favorable area for future exploration are still not well defined. Here we use the available high-resolution seismic lines, well and heat flow data in the Qiongdongnan Basin to investigate the issues through calculating the thickness of gas hydrate stability zone (GHSZ) and estimating the inventory.

2 GEOLOGICAL SETTING

The northern South China Sea (SCS) passive margin (Fig.2a) is formed under multiple-episodic rifting in the late Cretaceous to Oligocene (Ru and Pigott, 1986; Sun et al., 2021) prior to seafloor spreading in the Oligocene to early Miocene (Taylor and Hayes, 1983; Briais et al., 1993; Li et al., 2014). Several large sedimentary basins such as the Qiongdongnan and Zhujiang River Mouth Basins are developed along the margin (Fig.2a). In the post-spreading period, the margin is featured by fast

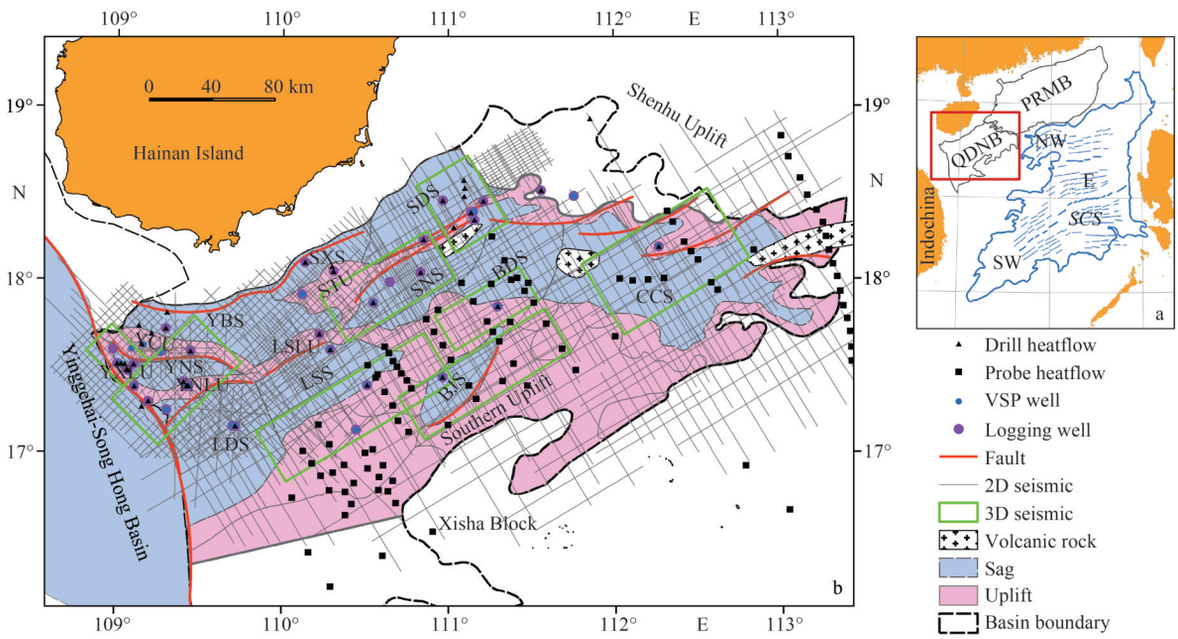

Fig.2 Locations of Qiongdongnan Basin (QDNB) and South China Sea (SCS) (a); structural units and dataset in the Qiongdongnan Basin (b)

In (a), E, NW, and SW denotes the east sub-basin, northwest sub-basin, and southwest sub-basin of the South China Sea oceanic basin, respectively. PRMB: Zhujiang River Mouth Basin. Gray lines are 500 seismic lines. In (b), red lines are faults. Green rectangles are 8 seismic patches. Blue dots are 21 VSP data. Purple dots are 38 logging data. Heat flow data are measured from drill sites (black triangles) and from seafloor heat flow probe stations (black solid square) (Wang et al., 2014; Zhao et al., 2018a, b). BJS: Beijiao Sub-basin; BDS: Baodao Sub-basin; CCS: Changchang Sub-basin; SNS: Songtao Nan Sub-basin; LSS: Lingshui Sub-basin; LDS: Ledong Sub-basin; LSLU: Lingshui Low Uplift; SDS: Songtao Dong Sub-basin; SXS: Songtao Xi Sub-basin; STU: Songtao Uplift; YBS: Yacheng Bei Sub-basin; YCU: Yacheng Uplift; YNLU: Yacheng Nan Low Uplift; YNS: Yacheng Nan Sub-basin; YXLU: Yacheng Xi Low Uplift.

basement subsidence and high sedimentation (Zhao et al., 2015, 2018b). In the west Qiongdongnan Basin, the sedimentation rate exceeds ~1 000 m/Ma since the Middle Pleistocene (1.8–0 Ma) (Fig.3b) (Zhao et al., 2015, 2018b).

The Qiongdongnan Basin covers an area of ca. 8.4×10^4 km^2 (Fig.2b). Water depths span from 100 to 2 500 m and increase toward southeast (Fig.3a). The basin started rifting in the middle Eocene (~45 Ma) and consists of three major structural units: the northern uplift, central depression, and southern uplift (Fig.2a). The central depression comprises the LDS, LSS, SNS, BDS, CCS, and BJS (Fig.2b), in which, the Cenozoic sediment reaches ~10 km thick (Fig.3c) (Zhao et al., 2015). The heat flow also increases from continental shelf to slope, which is ~50–70 mW/m^2 in the northern shelf and upper slope, ~70–85 mW/m^2 in the central depression, and ~85– 105 mW/m^2 in the eastern sub-basins (Wang et al., 2014).

3 DATA AND METHOD

3.1 Data

GHSZ is principally controlled by temperature and pressure conditions within sediment. Calculating the thickness of GHSZ thus requires bathymetry, sediment thickness, bottom water temperature, heat flow, and geothermal gradient. The first two data sets are obtained from high resolution, dense seismic grid, and industrial wells (Fig.2b) in courtesy of China National Offshore Oil Corporation (CNOOC) (Zhao et al., 2018b). The seismic data contains 500 seismic lines with a resolution of 1 km×1 km and 8 seismic patches, which were collected using a 7.5-km long streamer at a trace interval of ca. 12.5 m (Fig.2b). The industrial wells, consisting of 38 logging data and 21 vertical seismic profile (VSP) data, are used to constrain the strata ages, lithology and time-depth conversion (Zhao et al., 2018b). Under constraints of the seismic and well data, the bathymetry (Fig.3a) and sediment thickness since the Middle Pleistocene (1.8–0 Ma; Fig.3b) and during the Cenozoic (45–0 Ma; Fig.3c) are derived, respectively, on 10 666 grid nodal points.

Bottom water temperature, heat flow, and geothermal gradient are also key parameters controlling gas hydrate stability. The previously observed bottom water temperature versus water depth in the SCS region

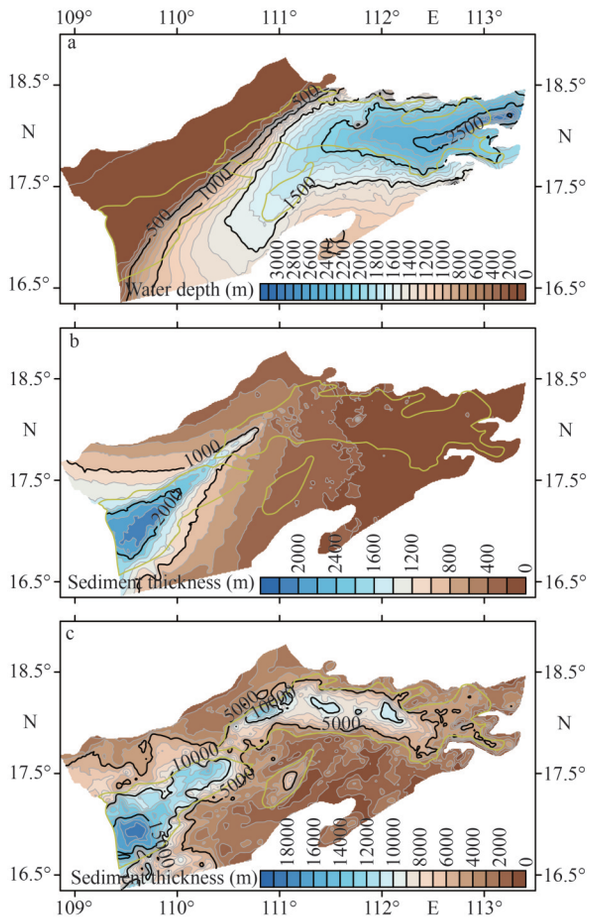

Fig.3 Seafloor topography showing increasing water depth southeastward from ~100 to 2 500 m (a); sediment thickness (in m) since the Middle Pleistocene (1.8–0 Ma) (b); sediment thickness (in m) during the Cenozoic (45–0 Ma) (c)

Yellow outline is the location of central depression.

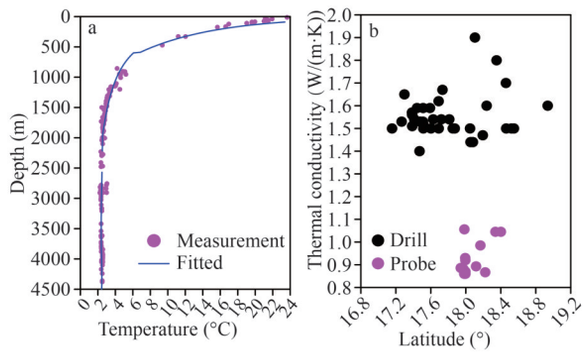

Fig.4 Observed bottom water temperature versus water depth (purple points) in the South China Sea (Yang et al., 2018) with the fitted curve (blue line) (Shi et al., 2015; Yang et al., 2018) (a); sediment thermal conductivity is ~1.4–1.8 W/(m·k) in drill sites and ~0.8–1.1 W/(m·k) in seafloor heat flow probe stations (see locations in Fig.2b) (Wang et al., 2014) (b)

(Fig.4a) (Yang et al., 2018) are used to fit the relationship between bottom water temperature and water depth, which is used to calculate the bottom water temperature in the Qiongdongnan Basin (Fig.5a). The measured heat flow (Fig.5b) and sediment thermal conductivity (Fig.4b) derived from 44 industrial drills in the shallow water and 110 seafloor heat flow probe stations in the deep water area (Wang et al., 2014) are applied to obtain the sediment geothermal gradients (Fig.5c) and temperature. The heat flow data has a resolution of ~2.6 drills per 1 000 km^2.

3.2 Calculating the thickness of gas hydrate stability zone (GHSZ)

Gas hydrates are stable at relatively low temperature and high pressure. A fourth order polynomial was provided to define the gas hydrate stability boundary (Miles, 1995):

$$P_b=2.8074023+aT+bT^2+cT^3+dT^4, \quad (1)$$

where a=1.559 474×10^{-1}; b=4.827 5×10^{-2}; c=-2.780 83×10^{-3}; d=1.592 2×10^{-4}; P_b is the pressure (in MPa) and T is the temperature (in °C).

Temperature in sediment is:

$$T_z=T_0+(\Delta T/\Delta z)z, \quad (2)$$

where T_z is sediment temperature (°C) at depth z (meter below seabed); T_0 is bottom water temperature (°C) at seabed; and $\Delta T/\Delta z$ is geothermal gradient within sediment.

Conversion between pressure (P_s, MPa) and depth (D, meter below sea level) in sediment is:

$$P_s=[(1+C_1)D+C_2D^2]\times10^{-2}, \quad (3)$$

where $C_1=[5.92+5.25\sin^2L]\times10^{-3}$, L is the latitude (in degree); $C_2=2.21\times10^{-6}$; $D=z_0+z$, z_0 is water depth below sea level (m).

Substituting Eq.2 into Eq.3 gives hydrostatic pressure-temperature relationship Eq.4 of the sediment.

$$P_s=[(1+C_1)(z_0+(T_z-T_0)\Delta z/\Delta T)+C_2(z_0+(T_z-T_0)\Delta z/\Delta T)^2]\times10^{-2}. \quad (4)$$

Simultaneously solving and comparing P_s and P_b can constrain the base of the gas hydrate stability and obtain the thickness of GHSZ in the Qiongdongnan Basin (Fig.6).

3.3 Calculating gas hydrate inventory (GHI)

A transport-reaction model was constructed to explore controlling factors on gas hydrate accumulation (Wallmann et al., 2006). On basis of a

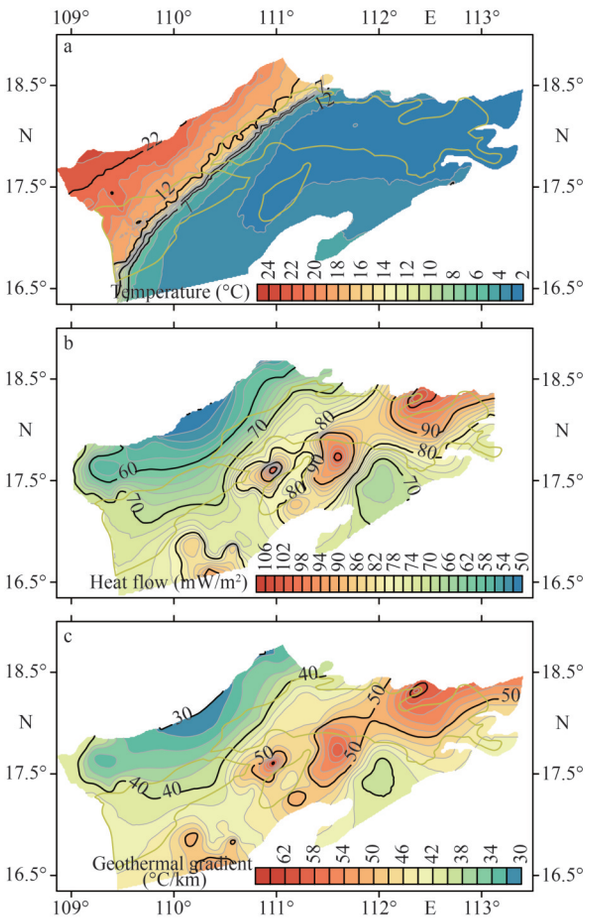

Fig.5 Bottom water temperature decreasing southeastward from 24 to 2 °C with increasing water depth (a); heat flow ranges between ~50 and 100 mW/m² (Wang et al., 2014) (b); the calculated geothermal gradient ranges between ~30 and 60 °C/km (c)

In (b), in the shelf and upper slope, the heat flow is ~50–70 mW/m². In the deep water, the heat flow is higher than 70 mW/m² with a remarkable zone of ~85–100 mW/m² trending northeast in the eastern sub-basins.

series of modelling, a transfer function (5) is given to estimate the GHI for completely compacting margin sediments (Wallmann et al., 2012):

$$\mathrm{GHI} = a \cdot L_{\mathrm{GHSZ}}^{b} \cdot \left(\mathrm{POC}_0 - \frac{c}{w_0^{d}} \right) \cdot \exp\left\{ -\left[e + f \cdot \ln\left(w_0 \right) \right]^2 \right\}, \quad (5)$$

where a=0.002 848±0.000 49; b=1.681±0.027; c=24.42±7.2; d=0.994 4±0.10; e=-1.441±0.19; f=0.392 5±0.032; GHI is gas hydrate inventory within GHSZ (in kg methane-C/m²); L_{GHSZ} is GHSZ thickness (in m), POC_0 (in wt%) and w_0 (in cm/ka) are POC concentration and burial velocity (cm/ka) in surface sediments. The function is valid for GHI≥0 over a range of L_{GHSZ}=0–1 000 m; w_0=10–150 cm/ka; and POC_0=0.2–5 wt%. Here the POC_0 is given a value of 5% to estimate the maximum value of GHI in the Qiongdongnan Basin (Fig.7).

4 RESULT AND DISCUSSION

4.1 Spatial distribution of GHSZ in the Qiongdongnan Basin

Natural gas hydrates are of highly interest to academia and industry due to implications for submarine geohazards, a future energy source (~10 times greater than conventional reserves), global climate change (methane is a greenhouse gas ~25 times more effective at raising temperature than CO_2) (Kennett and Stott, 1991; Dickens et al., 1995) and carbon cycle (occupying a third of the world's mobile organic carbon) (Beaudoin et al., 2014). Multidisciplinary hydrate investigations were conducted in the South China Sea, including the seismic survey, pressure and non-pressure coring, logging while drilling, in-situ temperature and permeability measurements, pore water sampling (Wang et al., 2011; Song et al., 2014; Zhang et al., 2015; Ye et al., 2019). These studies revealed widespread bottom simulating reflectors (BSRs), an important indicator of the base of GHSZ (John et al., 1991; Kvenvolden et al., 1993), in the offshore Taiwan Island (Liu et al., 2006; Lin et al., 2009), Zhujiang River Mouth Basin (Zhang et al., 2015; Qian et al., 2018; Li et al., 2020), and Qiongdongnan Basin (Figs.6–8) (Deng et al., 2021; Jiang et al., 2021), cored the disseminated and massive gas hydrate deposits (Wang et al., 2011; Zhang et al., 2015; Qian et al., 2018), and successfully performed the first test production in 2017 in the Shenhu area in the Zhujiang River Mouth Basin (Wu and Wang, 2018).

In the Qiongdongnan Basin, hydrate related gas chimneys (Fig.8) (Ye et al., 2019; Deng et al., 2021; Jiang et al., 2021) and active cold seeps due to methane leakage (Zhao et al., 2020) were also discovered, which indicate the occurrence of abundant gas hydrate deposit in the basin. Calculation of GHSZ thickness further reveals that the GHSZ thickness ranges mostly between ~200 and 400 m at water depths >500 m (Fig.6). The total gas hydrate inventory is ~6.5×10⁹ t carbon over an area of ~6×10⁴ km² (Fig.7). Furthermore, three areas including the lower uplift to the south of the LSS, the SNS and BDS, and the CCS are found to have a thick GHSZ of ~250–310 m, 250–330 m, and 350–400 m,

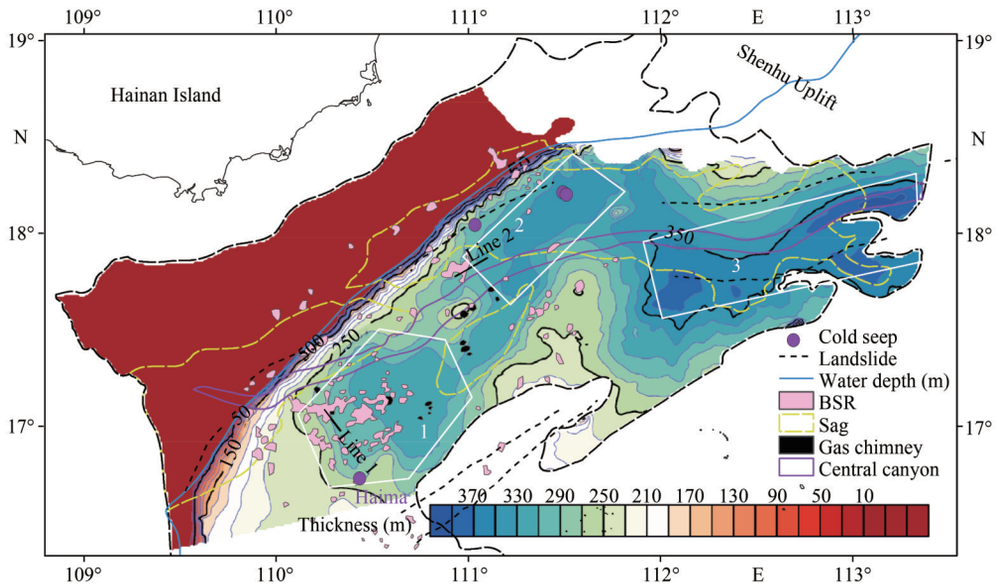

Fig.6 Spatial distribution of thickness (in m) of gas hydrate stability zone (GHSZ)

The GHSZ thickness of ~200–400 m occurs at water depths >500 m (thick blue line). The lower uplift to the south of the LSS (Area 1), the SNS and BDS (Area 2), and the CCS (Area 3) have the largest GHSZ thickness of ~250–310 m, 250–330 m, and 350–400 m, respectively. In the lower uplift to the south of the LSS, hydrate-related bottom simulating reflectors (BSRs) (Jiang et al., 2021), gas chimneys (Wang et al., 2018; Liao et al., 2021) and active cold seeps (Feng et al., 2018; Zhao et al., 2020) were revealed. In the SNS and BDS, gas hydrates were found distributed in a vertical chimney structure (Ye et al., 2019). Seismic lines 1 and 2 are shown in Fig.8.

respectively (Fig.6), where the estimated gas hydrate inventory all exceeds ~150 kg/m^2 (Fig.7).

The calculated GHSZ thickness is compared with the seismically measured GHSZ thickness along line 1 in the lower uplift to the south of the LSS and line 2 in the lower uplift to the south of SNS (see locations in Fig.6). The base of seismically interpreted GSHZ is constrained by BSRs (John et al., 1991; Kvenvolden et al., 1993). The thickness of GHSZ between seafloor and BSRs along lines 1 and 2 are derived on basis of the two-way travel time using a *P* velocity of ~2 500 km/s (Hyndman and Davis, 1992) (Fig.8). Results show that the calculated GHSZ thickness is consistent with the seismically measured

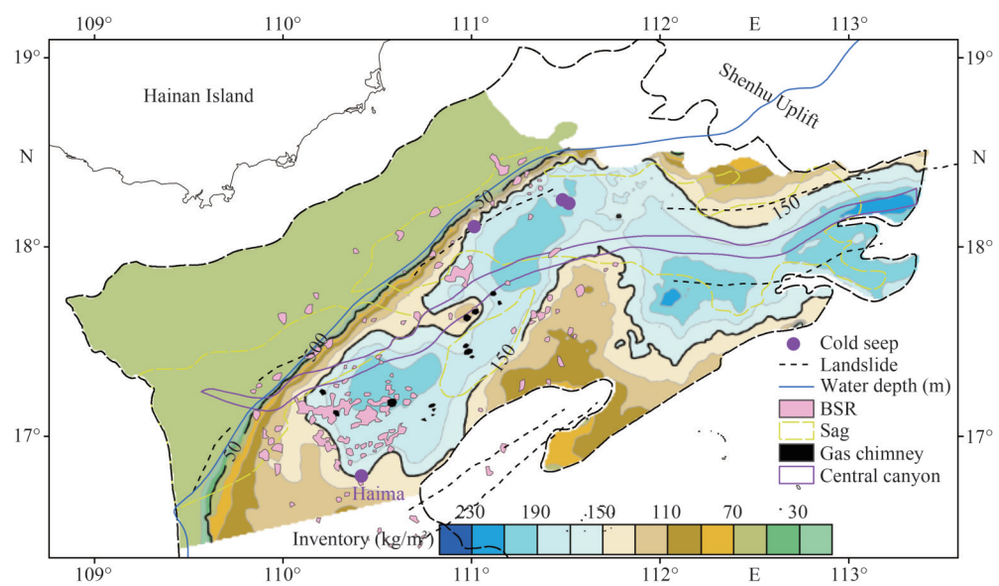

Fig.7 The gas hydrate inventory (GHI, kg/m^2) given the maximum POC$_0$ of 5%

The GHI exceeds 150 kg/m^2 in three areas: 1) the lower uplift to the south of the LSS, 2) the BDS and SNS, and 3) the CCS. The total gas hydrate inventory is ~6.5×10^9 t carbon over an area of ~6×10^4 km^2.

GHSZ thickness and the maximum deviation is less than ~25 m along lines 1 and 2 (Fig.8).

4.2 Main factor controlling GHSZ thickness in the Qiongdongnan Basin

GHSZ thickness depends on local sediment temperature-pressure conditions. Low bottom-water temperature, heat flow, geothermal gradient, and large bathymetry are in favor of thick GHSZ formation. In the Qiongdongnan Basin, gas hydrates stay stable at water depths >500 m (Fig.6). In these deep water area, bottom water temperature varies slightly and decreases with water depth from ~6–2 °C (Figs.5a & 6a) (Yang et al., 2018), which has thus little effects on GHSZ thickness. However, the measured heat flow increases with water depth. It is ~50–70 mW/m^2 in water depth <500 m, and ~70–100 mW/m^2 in water depth >500 m (Fig.5b)

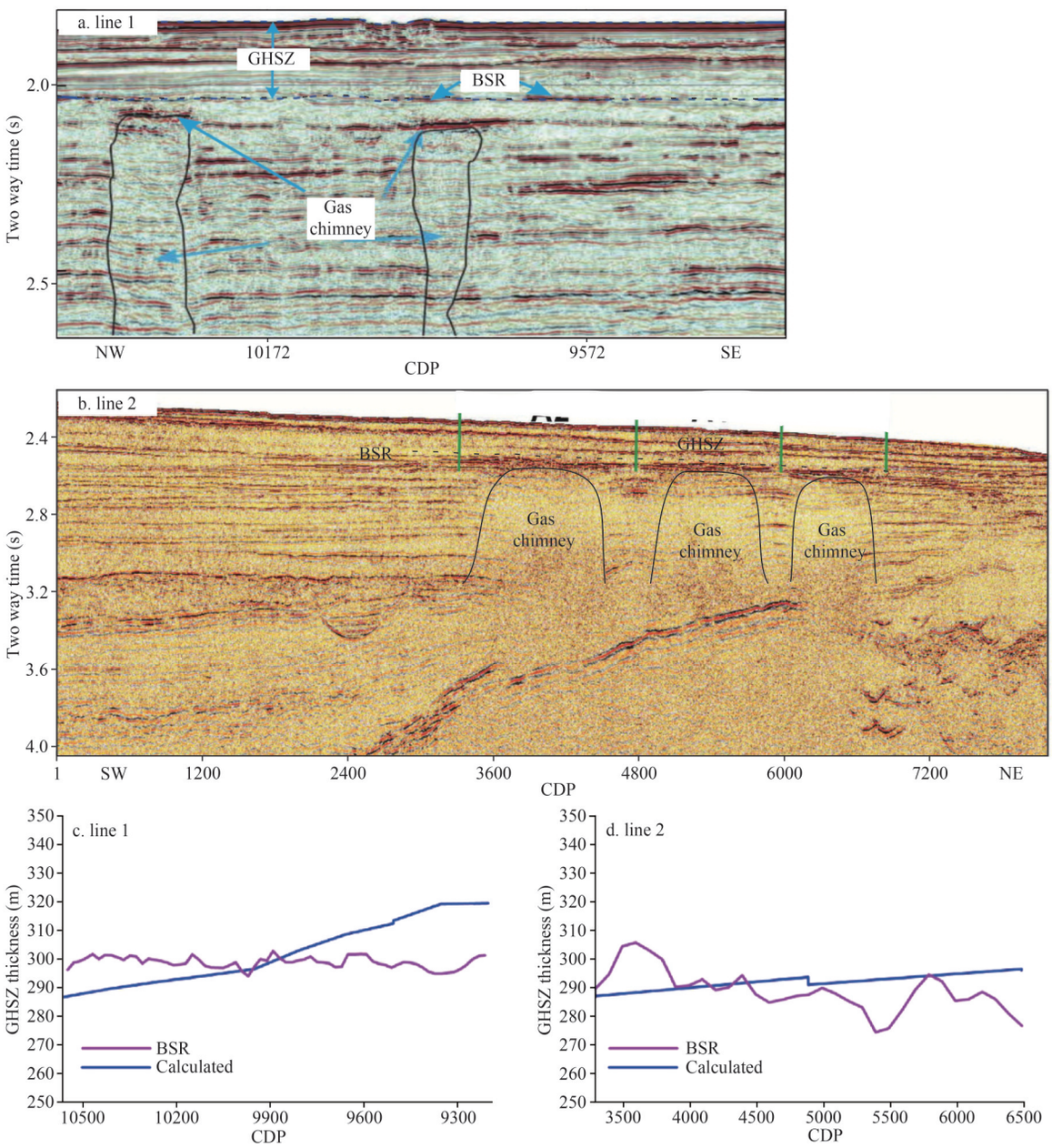

Fig.8 Interpreted gas chimneys, bottom simulating reflectors (BSR), and gas hydrate stability zone (GHSZ) along line 1 (modified from Jiang et al., 2021; see location in Fig.6) (a) and line 2 (modified from Deng et al., 2021; see location in Fig.6) (b); GHSZ thickness calculated in this paper and measured on basis of seismically interpreted BSR along line 1 (c) and line 2 (d)

(Wang et al., 2014), on basis of which, the calculated geothermal gradient also increases with water depth. It is ~30–40 °C/km in shallow water and ~40–60 °C/km in deep water (Fig.5c). High heat flow and geothermal gradient tend to reduce GHSZ thickness, while the thickest GHSZ of ~350–400 m still occurs in the CCS where the heat flow is the highest of 80–100 mW/m^2 and the water depth is the largest of ~2 400–3 000 m (Fig.6). It is obvious that water depth is a dominant factor in controlling GHSZ thickness in the Qiongdongnan Basin.

4.3 Favorable area for gas hydrate accumulation in the Qiongdongnan Basin

GHSZ provides potential space for gas hydrates but it cannot guarantee accumulation of gas hydrates (Burwicz et al., 2011). In addition to GHSZ, hydrate accumulation also relies on gas sources and transport systems, which are commonly grouped into two end members, the diffusion and venting systems (Su and Chen, 2006). In the diffusion system, two phases of water and hydrate reach thermodynamic equilibrium in GHSZ. Beneath the base of GHSZ, biogenic gas accumulates to form bottom simulating reflectors (BSR). However, the venting system is in thermodynamic unequilibrium and controlled by kinetics. It requires assistance of conduits, such as faults, diapirs and/or gas chimneys, to transport deep thermogenic gas to GHSZ, where three phases of water-hydrate-gas coexist. In the venting system, no BSR formed but mud volcanoes and pockmarks are usually observed at seafloor.

In the Qiongdongnan Basin, large GHSZ thickness occurs in three areas including the lower uplift to the south of the LSS, the SNS and BDS, and the CCS where water depths are ~1 000–1 600 m, 1 000–2 000 m, and 2 400–3 000 m, respectively (Fig.3a), and sediment thickness is respectively of ~500–1 500 m, 200–600 m, and 0–200 m since the middle Pleistocene (1.8–0 Ma) (Fig.3b). The lower uplift to the south of the LSS has relatively shallow water and high sedimentation rate (~270–830 m/Ma in 1.8–0 Ma) (Zhao et al., 2015). The rapid deposition with sufficient organic matters can provide biogenic gas to form diffusive hydrate in the GHSZ and the extensive hydrate-related BSRs which tend to cluster toward the sediment center (Fig.6) (Jiang et al., 2021). Due to rapid and persistent subsidence, the surrounding areas also have a thick Cenozoic sediment (~500–15 000 m, Fig.3) (Zhao et al., 2015). The syn-rifting Eocene-Early Oligocene organic matters are thus deep buried, over-matured and gas-produced, which is a thermogenic gas source (Zhu et al., 2011), but needs a channel to vertically migrate into the GHSZ. Previous studies showed that the Neogene polygonal faults (Wu et al., 2009; Wang et al., 2010), mud diapirs (Zhu et al., 2011), and gas chimneys (Wang et al., 2018; Jiang et al., 2021; Liao et al., 2021) are widely developed in the post-rifting strata, which can transport deep thermogenic gas to the GHSZ and seafloor to form hydrate, pockmarks (Wang et al., 2018), and active “Haima” cold seeps (Feng et al., 2018; Zhao et al., 2020). The methane carbon isotope composition of “Haima” cold seep also suggested a mixed gas source (Zhao et al., 2020). Therefore, the lower uplift to the south of the LSS has rich biogenic and thermogenic gas supplies (Zhao et al., 2020) and excellent transport systems (faults, diapirs, and gas chimneys). The coarse sediment with relatively high permeability in the low uplift is thus favorable for hydrate accumulation and the lower uplift is a priority for future exploration, especially where pockmarks (Wang et al., 2018) and active cold seeps (Feng et al., 2018; Zhao et al., 2020) are discovered (Fig.6). Moreover, the seismically identified landslides (Ma, 2014) are far away located from seafloor pockmarks and cold seeps (Fig.6), which are probably unrelated to methane release in the hydrate province.

The SNS and BDS have the sedimentation rate of ~110–330 m/Ma in 1.8–0 Ma (Zhao et al., 2015) where the gas hydrate was also found to distribute within a vertical chimney structure (Figs.6 & 8) (Ye et al., 2019; Deng et al., 2021), implying another potential reservoir for gas hydrate accumulation. However, in the CCS, the sedimentation is extremely low of 0–110 m/Ma in 1.8–0 Ma (Zhao et al., 2015), probably indicating insufficient organic matters available for microbial methane formation although the calculated GHSZ thickness is the largest of ~350–400 m (Fig.6).

5 CONCLUSION

The thickness of gas hydrate stability zone (GHSZ) in the Qiongdongnan Basin ranges mostly between ~200 and 400 m at water depths >500 m. The gas hydrate inventory is ~6.5×10^9 t carbon over an area of ~6×10^4 km^2. Three areas including the lower uplift to the south of the Lingshui sub-basin, the Songnan and Baodao sub-basins, and the Changchang sub-basin have a thick GHSZ of ~250–310 m, 250–330 m, and 350–400 m, respectively, where water depths are ~1 000–1 600 m, 1 000–2 000 m,

and 2 400–3 000 m, respectively. In these deep waters, the bottom water temperatures fall in a narrow range of ~4 and 2 °C. However, the heat flow increases with water depth and reaches a peak of ~80–100 mW/m^2 in the deepest water area of Changchang sub-basin. High heat flow tends to reduce GHSZ thickness, however, the thickest GHSZ still occurs in the Changchang sub-basin, highlighting the role of water depth in controlling GHSZ. The lower uplift to the south of the Lingshui sub-basin has high deposition rate (~270–830 m/Ma in 1.8–0 Ma), thick Cenozoic sediment, rich biogenic and thermogenic gas supplies and excellent transport systems (faults, diapirs, and gas chimneys), enabling it a favorable area for hydrate accumulation where hydrate-related bottom simulating reflectors, gas chimneys, and active cold seeps were widely revealed.

6 DATA AVAILABILITY STATEMENT

All data generated and/or analyzed during this study are available from the corresponding author upon reasonable request.

7 ACKNOWLEDGMENT

Thank two anonymous reviewers for valuable and constructive comments with which this manuscript is improved. The seismic and well data are provided by the China National Offshore Oil Corporation.

References

Beaudoin Y C, Waite W F, Boswell R et al. 2014. Frozen heat: a UNEP global outlook on methane gas hydrates. United Nations Environment Programme, **1**: 1-80.

Briais A, Patriat P, Tapponnier P. 1993. Updated interpretation of magnetic anomalies and seafloor spreading stages in the South China Sea: implications for the tertiary tectonics of Southeast Asia. *Journal of Geophysical Research*: *Solid Earth*, **98**(B4): 6299-6328, https://doi.org/10.1029/92JB02280.

Burwicz E B, Rüpke L H, Wallmann K. 2011. Estimation of the global amount of submarine gas hydrates formed via microbial methane formation based on numerical reaction-transport modeling and a novel parameterization of Holocene sedimentation. *Geochimica et Cosmochimica Acta*, **75**(16): 4562-4576, https://doi.org/10.1016/j.gca.2011.05.029.

Claypool G E, Kaplan I R. 1974. The origin and distribution of methane in marine sediments. *In*: Kaplan I R ed. Natural Gases in Marine Sediments. Springer, Boston. p. 99-139, https://doi.org/10.1007/978-1-4684-2757-8_8.

Deng W, Liang J Q, Zhang W et al. 2021. Typical characteristics of fracture-filling hydrate-charged reservoirs caused by heterogeneous fluid flow in the Qiongdongnan Basin, northern South China Sea. *Marine and Petroleum Geology*, **124**: 104810, https://doi.org/10.1016/j.marpetgeo.2020.104810.

Dickens G R, O'Neil J R, Rea D K et al. 1995. Dissociation of oceanic methane hydrate as a cause of the carbon isotope excursion at the end of the Paleocene. *Paleoceanography*, **10**(6): 965-971, https://doi.org/10.1029/95pa02087.

Feng D, Qiu J W, Hu Y et al. 2018. Cold seep systems in the South China Sea: an overview. *Journal of Asian Earth Sciences*, **168**: 3-16, https://doi.org/10.1016/j.jseaes.2018.09.021.

Flögel S, Wallmann K, Poulsen C J et al. 2011. Simulating the biogeochemical effects of volcanic CO_2 degassing on the oxygen-state of the deep ocean during the Cenomanian/Turonian Anoxic Event (OAE**2**). *Earth and Planetary Science Letters*, **305**(3-4): 371-384, https://doi.org/10.1016/j.epsl.2011.03.018.

Hammerschmidt E G. 1934. Formation of gas hydrates in natural gas transmission lines. *Industrial & Engineering Chemistry*, **26**(8): 851-855, https://doi.org/10.1021/ie50296a010.

Hollister C D, Ewing J I, Habib D et al. 1972. Initial reports of the deep sea drilling project, V. XI: Washington, D.C., U.S. Govt. Printing Office, p.1-1077, https://doi.org/10.2973/dsdp.proc.11.1972.

Hyndman R D, Davis E E. 1992. A mechanism for the formation of methane hydrate and seafloor bottom-simulating reflectors by vertical fluid expulsion. *Journal of Geophysical Research*: *Solid Earth*, **97**(B5): 7025-7041, https://doi.org/10.1029/91JB03061.

Jiang D C, Liu R, Zhao X M et al. 2021. Dynamic migration of gas hydrate stability zone in the deep water areas of the Qiongdongnan basin since Pliocene and its distribution pattern. *Marine Geology Frontiers*, **37**(7): 43-51, https://doi.org/10.16028/j.1009-2722.2021.094. (in Chinese with English abstract)

John J M, Myung W L, Roland V H. 1991. An analysis of a seismic reflection from the base of a gas hydrate zone, offshore Peru. *AAPG Bulletin*, **75**(5): 910-924, https://doi.org/10.1306/0C9B288F-1710-11D7-8645000102C1865D.

Kennett J P, Stott L D. 1991. Abrupt deep-sea warming, palaeoceanographic changes and benthic extinctions at the end of the Palaeocene. *Nature*, **353**(6341): 225-229, https://doi.org/10.1038/353225a0.

Kvenvolden K A. 1993. Gas hydrates—geological perspective and global change. *Reviews of Geophysics*, **31**(2): 173-187, https://doi.org/10.1029/93RG00268.

Kvenvolden K A, Ginsburg G D, Soloviev V A. 1993. Worldwide distribution of subaquatic gas hydrates. *Geo-Marine Letters*, **13**(1): 32-40, https://doi.org/10.1007/BF01204390.

Li C F, Xu X, Lin J et al. 2014. Ages and magnetic structures of the South China Sea constrained by deep tow magnetic surveys and IODP Expedition 349. *Geochemistry*, *Geophysics*, *Geosystems*, **15**(12): 4958-4983, https://doi.

org/10.1002/2014GC005567.

Li J, He M, Yan C Z et al. 2020. Seismic anomalies of gas hydrate-bearing sediments in the Jieyang sag, northern slope of South China Sea. *Oceanologia et Limnologia Sinica*, **51**(2): 274-282, https://doi.org/10.11693/hyhz20191100218.

Liao J, Luo J S, Song P et al. 2021. Genetic types and development characteristics of gas chimneys in the Qiongdongnan basin and their control on hydrate accumulation. *Marine Geology Frontiers*, **37**(7): 33-42, https://doi. org/10.16028/j.1009-2722.2021.119. (in Chinese with English abstract)

Lin C C, Lin A T S, Liu C S et al. 2009. Geological controls on BSR occurrences in the incipient arc-continent collision zone off southwest Taiwan. *Marine and Petroleum Geology*, **26**(7): 1118-1131, https://doi.org/10.1016/j.marpetgeo.2008.11.002.

Liu C S, Schnurle P, Wang Y et al. 2006. Distribution and characters of gas hydrate offshore of southwestern Taiwan. *Terrestrial*, *Atmospheric and Oceanic Sciences*, **17**(4): 615-644, https://doi.org/10.3319/TAO.2006.17.4.615(GH).

Ma Y. 2014. Study of Submarine Landslides and Trigger Mechanism along the Continental Slope of the Northern South China Sea. Ocean University of China, Qingdao, p.1-112. (in Chinese with English abstract)

Marchetti C. 1985. Nuclear plants and nuclear niches—on the generation of nuclear energy during the last Twenty years. *Nuclear Science and Engineering*, **90**(4): 521-526, https://doi.org/10.13182/NSE85-A18502.

Miles P R. 1995. Potential distribution of methane hydrate beneath the European continental margins. *Geophysical Research Letters*, **22**(23): 3179-3182, https://doi.org/10.1029/95GL03013.

Milkov A V. 2004. Global estimates of hydrate-bound gas in marine sediments: how much is really out there? *Earth-Science Reviews*, **66**(3-4): 183-197, https://doi.org/10.1016/j.earscirev.2003.11.002.

Paull C K, Brewer P G, Ussler W et al. 2002. An experiment demonstrating that marine slumping is a mechanism to transfer methane from seafloor gas-hydrate deposits into the upper ocean and atmosphere. *Geo-Marine Letters*, **22**(4): 198-203, https://doi.org/10.1007/s00367-002-0113-y.

Qian J, Wang X J, Collett T S et al. 2018. Downhole log evidence for the coexistence of structure II gas hydrate and free gas below the bottom simulating reflector in the South China Sea. *Marine and Petroleum Geology*, **98**: 662-674, https://doi.org/10.1016/j.marpetgeo.2018.09.024.

Ripmeester J A, Tse J S, Ratcliffe C I et al. 1987. A new clathrate hydrate structure. *Nature*, **325**(6100): 135-136, https://doi.org/10.1038/325135a0.

Ru K, Pigott J D. 1986. Episodic rifting and subsidence in the South China Sea. *AAPG Bulletin*, **70**(9): 1136-1155, https://doi.org/10.1306/94886A8D-1704-11D7-8645000102C1865D.

Shi X B, Wang Z F, Jiang H Y et al. 2015. Vertical variations of geothermal parameters in rifted basins and heat flow distribution features of the Qiongdongnan Basin. *Chinese Journal of Geophysics*, **58**(3): 939-952, https://doi.org/10.6038/cjg20150320. (in Chinese with English abstract)

Sloan E D Jr, Koh C A. 2007. Clathrate Hydrates of Natural Gases. 3rd edn. CRC Press, Boca Raton, https://doi.org/10.1201/9781420008494.

Song Y C, Yang L, Zhao J F et al. 2014. The status of natural gas hydrate research in China: a review. *Renewable and Sustainable Energy Reviews*, **31**: 778-791, https://doi.org/10.1016/j.rser.2013.12.025.

Stackelberg M V. 1949. Feste gashydrate. *Naturwissenschaften*, **36**(12): 359-362, https://doi.org/10.1007/BF00627172.

Su Z, Chen D F. 2006. Types of gas hydrates and their characteristics in marine environments. *Geotectonica et Metallogenia*, **30**(2): 256-264, https://doi.org/10.3969/j.issn.1001-1552.2006.02.016. (in Chinese with English abstract)

Sun L H, Sun Z, Zhang Y Y et al. 2021. Multi-stage carbonate veins at IODP Site U1504 document early cretaceous to early cenozoic extensional events on the South China Sea margin. *Marine Geology*, **442**: 106656, https://doi.org/10.1016/j.margeo.2021.106656.

Taylor B, Hayes D E. 1983. Origin and History of the South China Sea Basin. *In*: Hayes D E ed. The Tectonic and Geologic Evolution of Southeast Asian Seas and Islands: Part 2. American Geophysical Union, Washington, p.23-56, https://doi.org/10.1029/GM027p0023.

Wallmann K, Aloisi G, Haeckel M et al. 2006. Kinetics of organic matter degradation, microbial methane generation, and gas hydrate formation in anoxic marine sediments. *Geochimica et Cosmochimica Acta*, **70**(15): 3905-3927, https://doi.org/10.1016/j.gca.2006.06.003.

Wallmann K, Pinero E, Burwicz E et al. 2012. The global inventory of methane hydrate in marine sediments: a theoretical approach. *Energies*, **5**(7): 2449-2498, https://doi.org/10.3390/en5072449.

Wang J L, Wu S G, Kong X et al. 2018. Subsurface fluid flow at an active cold seep area in the Qiongdongnan Basin, northern South China Sea. *Journal of Asian Earth Sciences*, **168**: 17-26, https://doi.org/10.1016/j.jseaes.2018.06.001.

Wang X J, Hutchinson D R, Wu S G et al. 2011. Elevated gas hydrate saturation within silt and silty clay sediments in the Shenhu area, South China Sea. *Journal of Geophysical Research*: *Solid Earth*, **116**(B5): B05102, https://doi.org/10.1029/2010JB007944.

Wang X J, Wu S G, Wang D W et al. 2010. The role of polygonal faults in fluid migration and gas hydrate reservoir forming in southeast Hainan Basin. *Oil Geophysical Prospecting*, **45**(1): 122-128, https://doi.org/10.1016/S1872-5813(11)60005-4. (in Chinese with English abstract)

Wang Z F, Shi X B, Yang J et al. 2014. Analyses on the tectonic thermal evolution and influence factors in the deep-water Qiongdongnan Basin. *Acta Oceanologica Sinica*, **33**(12): 107-117, https://doi. org/10.1007/s13131-014-0580-9.

Westbrook G K, Thatcher K E, Rohling E J et al. 2009. Escape of methane gas from the seabed along the West Spitsbergen continental margin. *Geophysical Research*

Letters, **36**(15): L15608, https://doi.org/10.1029/2009GL039191.

Wu S G, Sun Q L, Wu T Y et al. 2009. Polygonal fault and oil-gas accumulation in deep-water area of Qiongdongnan Basin. *Acta Petrolei Sinica*, **30**(1): 22-26, 32, https://doi.org/10.7623/syxb200901005. (in Chinese with English abstract)

Wu S G, Wang J L. 2018. On the China's successful gas production test from marine gas hydrate reservoirs. *Chinese Science Bulletin*, **63**(1): 2-8, https://doi.org/10.1360/N972017-00645. (in Chinese with English abstract)

Yang X Q, Shi X B, Zhao J F et al. 2018. Bottom water temperature measurements in the South China Sea, eastern Indian Ocean and western Pacific Ocean. *Journal of Tropical Oceanography*, **37**(5): 86-97, https://doi.org/10.11978/2017113.

Ye J L, Wei J G, Liang J Q et al. 2019. Complex gas hydrate system in a gas chimney, South China Sea. *Marine and Petroleum Geology*, **104**: 29-39, https://doi.org/10.1016/j.marpetgeo.2019.03.023.

Zhang G X, Liang J Q, Lu J A et al. 2015. Geological features, controlling factors and potential prospects of the gas hydrate occurrence in the east part of the Pearl River Mouth Basin, South China Sea. *Marine and Petroleum Geology*, **67**: 356-367, https://doi.org/10.1016/j.marpetgeo.2015.05.021.

Zhao J, Liang Q Y, Wei J G et al. 2020. Seafloor geology and geochemistry characteristic of methane seepage of the "Haima" cold seep, northwestern slope of the South China Sea. *Geochimica*, **49**(1): 108-118, https://doi.org/10.19700/j.0379-1726.2020.01.009. (in Chinese with English abstract)

Zhao Z X, Sun Z, Liu J B et al. 2018a. The continental extension discrepancy and anomalous subsidence pattern in the western Qiongdongnan Basin, South China Sea. *Earth and Planetary Science Letters*, **501**: 180-191, https://doi.org/10.1016/j.epsl.2018.08.048.

Zhao Z X, Sun Z, Sun L T et al. 2018b. Cenozoic tectonic subsidence in the Qiongdongnan Basin, northern South China Sea. *Basin Research*, **30**(S1): 269-288, https://doi.org/10.1111/bre.12220.

Zhao Z X, Sun Z, Wang Z F et al. 2015. The high resolution sedimentary filling in Qiongdongnan Basin, Northern South China Sea. *Marine Geology*, **361**: 11-24, https://doi.org/10.1016/j.margeo.2015.01.002.

Zhu J T, Pei J X, Sun Z P et al. 2011. Feature of neotectonism and its control on late hydrocarbon accumulation in Qiongdongnan Basin. *Natural Gas Geoscience*, **22**(4): 649-656, https://doi.org/10.11764/j.issn.1672-1926.2011.04.649. (in Chinese with English abstract)